ARTICLE IN PRESS

Available online at www.sciencedirect.com
SCIENCE DIRECT®

Solar Energy xxx (2006) xxx–xxx

SOLAR ENERGY

www.elsevier.com/locate/solener

Optical characterization of polysilicon thin films for solar applications

J. Müllerová [a,*], S. Jurečka [a], P. Šutta [b]

[a] Department of Engineering Fundamentals, Faculty of Electrical Engineering, University of Žilina, 031 01 Liptovský Mikuláš, Slovakia
[b] University of West Bohemia, New Technologies—Research Centre, Univerzitní 8, 306 14 Plzeň, Czech Republic

Received 16 June 2005; accepted 18 October 2005

Communicated by: Associate Editor Arturo Morales-Acevedo

Abstract

We report on the results of the investigation of optical properties and structure of PECVD deposited thin films of hydrogenated polysilicon determined by UV–Vis and IR spectroscopy. The influence of the hydrogen dilution of silane plasma at the PEVCD deposition on the film properties was investigated. The refractive index, the optical band gap energy and the microstructure of hydrogen and oxygen were analysed. The changes are discussed and correlated with the structure, the changes of the surface morphology and the hydrogen to silicon bonding. The optical band gap becomes larger than that of the undiluted sample. The results show that at dilution between 20 and 30 the transition between amorphous and crystalline phase occurs and the sample becomes a mixture of amorphous, polycrystalline phase with nano-sized grains and voids with decreasing hydrogen concentration. The presence of interstitial oxygen and oxygen bonded in surface Si–OH groups was detected.

Keywords: Polycrystalline; Si:H; Dilution

1. Introduction

Amorphous hydrogenated silicon (a-Si:H) and polycrystalline hydrogenated silicon (polysilicon Si:H) have become distinguished materials for thin film photovoltaics, microelectronics and optoelectronics. Solar applications of a-Si:H are limited due to the metastable defect creation, the so-called Staebler–Wronski effect (Staebler and Wronski, 1977). Much success has been achieved towards reducing the metastability and understanding its microscopic origin, especially in conventional plasma-enhanced chemical vapour deposition (PECVD) and hot-wire assisted chemical vapour deposition (HWCVD) (e.g., Brügemann et al., 1999; Nádaždy et al., 2002; Persheyev et al., 2004; Reynolds et al., 2005). PECVD is the most often used technique to deposit Si:H thin films with tailored structure and physical properties for photovoltaics and optoelectronics. However, the influence of the deposition conditions, the film thickness and the substrate on the microstructure, electrical and optical properties is still under exten-

* Corresponding author. Tel.: +421 960 4264 65; fax: +421 415 1315 15.
E-mail address: mullerova@lm.utc.sk (J. Müllerová).

0038-092X/$ - see front matter © 2005 Elsevier Ltd. All rights reserved.
doi:10.1016/j.solener.2005.10.009

Nomenclature

AFM	atomic force microscopy
A_x	vibrational mode proportionality constant (cm^{-2})
a-Si:H	amorphous hydrogenated silicon
C	hydrogen concentration
c_O	parameter related to oxygen concentration
D	dilution (hydrogen H_2 to silane SiH_4 gas flow)
E	photon energy (eV)
E_g	optical band gap energy (eV)
eV	electronvolt
FTIR	Fourier transform infrared
HWCVD	hot-wire assisted chemical vapour deposition
I	intensity
IR	infrared
N	density of hydrogen atoms (m^{-3})
N_{int}	total atomic density (m^{-3})
PECVD	plasma-enhanced chemical vapour deposition
rms	root mean square
r_s	ratio of absorption coefficients
Si:H	hydrogenated silicon
SiH_4	silane
SiH_x	silicon hydride
Si–OH	silanol groups
UV–Vis	ultraviolet and visible
XRD	X-ray diffraction
ZnSe	zinc selenide

Greek letters

α	absorption coefficient (m^{-1})
μ	microstructure factor
$\bar{\nu}$	wavenumber (cm^{-1})

Subscript

x	number of hydrogen atoms in silicon hydride SiH_x

sive study. The so-called protocrystalline Si, i.e., amorphous Si near and above the onset of microcrystallinity, attracts attention. The films prepared at the amorphous-to-crystalline phase boundary consisting of small crystallites of 10–100 nm embedded in a-Si network are recommended for manufacturing more stable solar cells (Koval et al., 1999; Wronski et al., 2002). As material properties are dependent on deposition conditions, systematic analysis is necessary to understand and control them. This work deals with spectroscopic studies of optical properties and of hydrogen and oxygen microstructure in the Si:H thin films deposited by PECVD on glass from hydrogen diluted silane plasma. As the structure of a thin film is manifested in the optical properties, the optical characterization is a valuable tool to complete the knowledge about structure collected by means e.g., X-ray diffraction (XRD) or Raman spectroscopy.

2. Experimental details

Undoped Si:H thin films of the approximately same thickness ~400 nm were deposited at the Delft University of Technology, the Netherlands, on clean Corning 1737 glass substrates by 13.5 MHz rf excited parallel plate PECVD industrial deposition system (rf power 13.5 W). The deposition was performed at the substrate temperature 194 °C and the total chamber pressure 200 Pa from hydrogen (H_2) to silane (SiH_4) plasma under varied H_2/SiH_4 gas flow (the dilution D). Besides this deposition parameter, also SiH_4 concentration defined as the ratio of $SiH_4/(H_2 + SiH_4)$ gas flows is often used.

UV–Vis transmittance spectral measurements were performed with Pye Unicam/Philips PU 8800 spectrophotometer at nearly normal incidence. The probed sample areas were ~0.2 cm^2. FTIR–DIGILAB FTS 3000MX Excalibur spectrophotometer in the internal HATR (horizontal attenuated total reflection) mode with ZnSe crystal was used to measure the infrared spectral absorbance.

The samples under study are described in Table 1 with some results of the structure reported recently elsewhere (Müllerová et al., 2005). According to XRD and Raman spectroscopy, amorphous phase prevails in films prepared at $D < 30$, but additional hydrogen at the deposition favours the crystallisation. XRD scans of the films deposited at $D \geqslant 30$ show the presence of diffraction lines ascribed to silicon (111), (220) and (311). Films deposited at $D \geqslant 30$ are apparently mixed-phase materials consisting of nano-crystallites embedded into amor-

Table 1
Samples under study

	Dilution D	SiH_4 concentration (%)	Thickness (nm)	Crystalline fraction[a] (%)	Average grain size[b] (nm)	Average grain size[a] (nm)
Reference	0	100	390	–	–	–
#1	10	9.1	394	–	–	–
#2	20	4.8	385	–	–	–
#3	30	3.2	388	61	10	5
#4	40	2.4	402	73	10	7
#5	50	2.0	397	82	40	9

[a] Determined from Raman spectra.
[b] Determined from XRD measurements.

phous matrix. The size of grains was determined as the size of coherently diffracting domains from the broadening of the diffraction lines by the procedure described by van Zutphen et al. (van Zutphen et al., 2001) and also from the Raman spectra according to the position of the peak at $\sim 520\ cm^{-1}$ belonging to the crystalline Si (Park and Rhee, 2001). The results are in Table 1. The macrostress analysis according to XRD scans showed that the films are predominantly under tensile stress (Müllerová et al., 2005).

The knowledge of microstructure can be correlated with the surface morphology investigated by the atomic force microscope NT–MDT SPM Solver P7 LS measuring in air in the contact repulsive mode with the lateral resolution of ~1–2 nm and the vertical resolution 0.01 nm. Surface analysis shows microcrystalline features appearing on the surface with increasing dilution as can be seen in the three-dimensional AFM images of the $1 \times 1\ \mu m^2$ sample frames in Fig. 1(a)–(c). The sample in Fig. 1(a) is still a-Si:H, the sample in Fig. 1(b) near to the protocrystalline regime and that in Fig. 1(c) polysilicon. The rms roughness acquired by the AFM data shows the maximum at $D \sim 30$ at which for the samples under study the amorphous-to-crystalline transition may be expected (Fig. 7(b)). The surface features seen by AFM are thought to be polycrystalline conglomerates of nano-sized crystalline grains seen by Raman spectroscopy or XRD as has been reported before (e.g., Kočka et al., 2004). The lateral dimensions of the largest features are 200–250 nm for the film prepared at $D = 30$ (Fig. 1(b)). The features are enveloped by amorphous tissue. With D increasing over this value the lateral size of features declines (e.g., ~100 nm in Fig. 1(c) for the sample #5 at $D = 50$). The surface features finally touch to form smoother surface (Fig. 1(c)).

3. Optical properties

The optical properties—the refractive index and the Tauc's optical band gap in general depend on the content of silicon, hydrogen and microvoids in the films. The optical properties were determined from transmittance spectra (Fig. 2) by the procedure based on the model of a quasi-ideal single homogeneous layer with smooth parallel interfaces on the thick incoherent substrate (Müllerová et al., 2003). Optical properties were extracted from the experimental transmittance by the optimization method based on the genetic algorithm optimisation procedure (Jurečka et al., 2003) by point-to-point processing without dispersion model. Spectral refractive indices of the samples are in Fig. 3. The refractive index at each wavelength decreases with increasing dilution owing to the increasing degree of the crystallinity and the decreasing density of films prepared at higher dilution. We deduce that this decrease is probably due to the voids.

The values of the optical band gap energy E_g were found from the plot of $(\alpha E)^{1/2}$ (α is the absorption coefficient, E the photon energy) versus photon energy E extrapolated to zero absorption. The absorption coefficients α were deduced from transmittance spectra in the vicinity of the absorption edge region in the interference free zone. Fig. 4 shows the relationship between the optical band gap and the dilution. The optical band gaps ~1.7–1.9 eV are typical for undoped silicon. It is obvious that the dilution opens the optical band gap with respect to reference sample of about 0.25 eV. Besides this, similar optical properties of the films prepared at dilutions $D = 40$ and 50 were observed. This is thought to be due to the stabilisation in the evolution of the network structure.

The hydrogen content is well known to affect the apparent band gap of a-Si:H. Hydrogen atoms

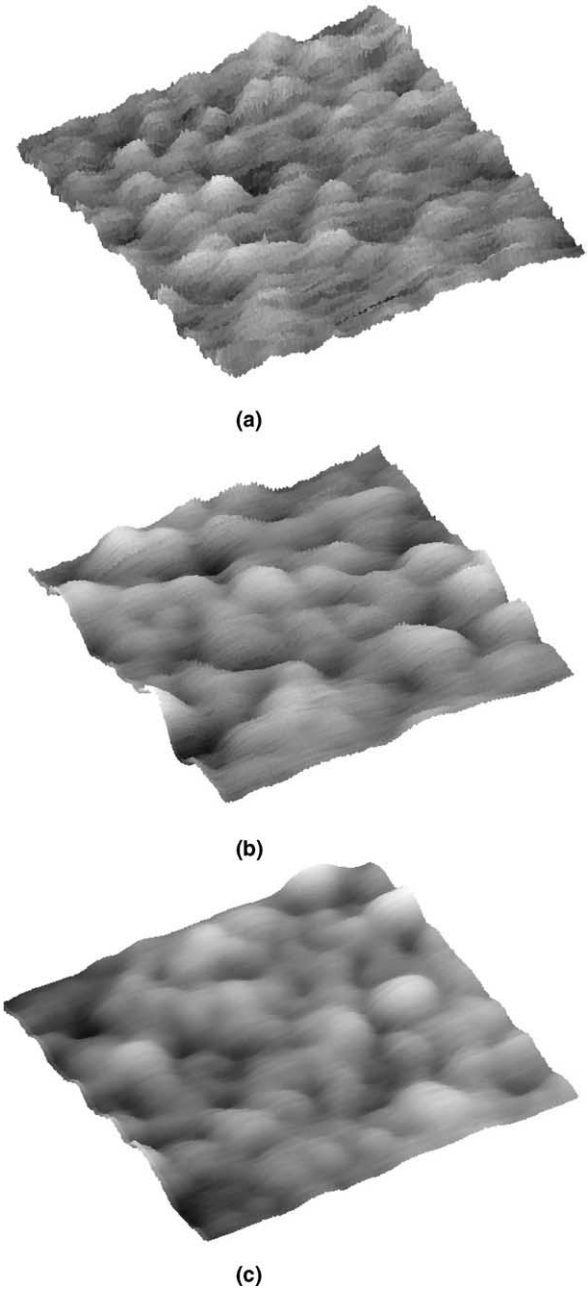

Fig. 1. Three-dimensional AFM images of the $1 \times 1\ \mu m^2$ frames of the deposited Si:H thin films. (a) The sample #2 deposited at the dilution 20, rms surface roughness 1.013 nm. (b) The sample #3 deposited at the dilution 30, rms surface roughness 3.629 nm. (c) The sample #5 deposited at the dilution 50, rms surface roughness 5.021 nm.

remove dangling bonds and thus reduce band tails increasing apparently the band gap. The increase of E_g at the amorphous-to-crystalline boundary is induced by the appearance of indirect gap electronic structure (gap near 3.3 eV) of the crystalline silicon.

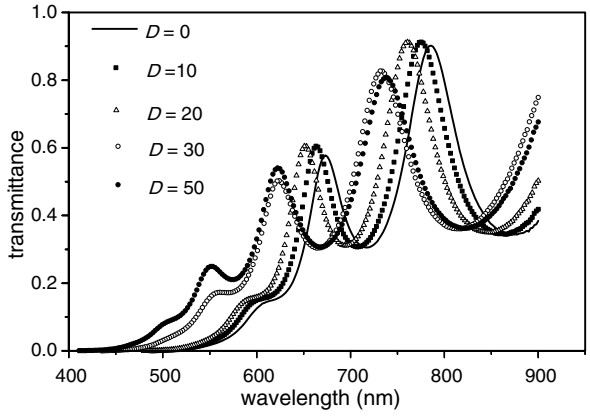

Fig. 2. Spectral transmittance of the samples deposited at the dilutions 10, 20, 30, and 50.

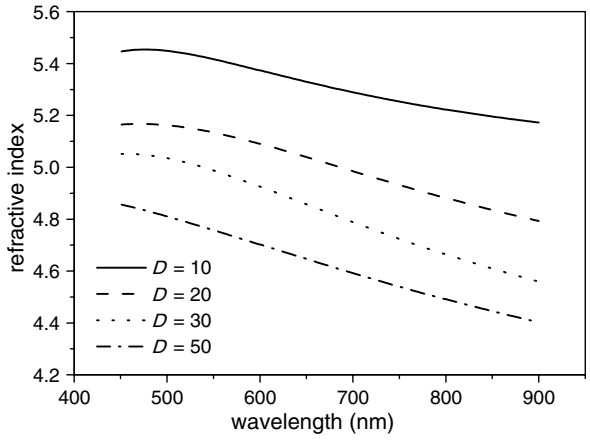

Fig. 3. Refractive index as a function of wavelength of samples deposited at the dilutions 10, 20, 30, and 50.

Thus, the samples prepared at $D \geqslant 30$ are polysilicon composed of grains and grain boundaries formed by amorphous Si and voids. Otherwise, polycrystalline films with voids are less homogeneous and non-homogeneity as well as the surface roughness should be taken into consideration. Nevertheless, the refractive indices reported here and extracted using a quasi-ideal film model could be considered as media effective values.

4. Microstructure of hydrogen and oxygen

FTIR absorbance spectra exhibit a number of absorption peaks corresponding to Si:H or Si–O bonds which assignments to the vibrational modes are in Table 2 (Gracin et al., 1995). Background subtracted FTIR spectra in extended wavenumber

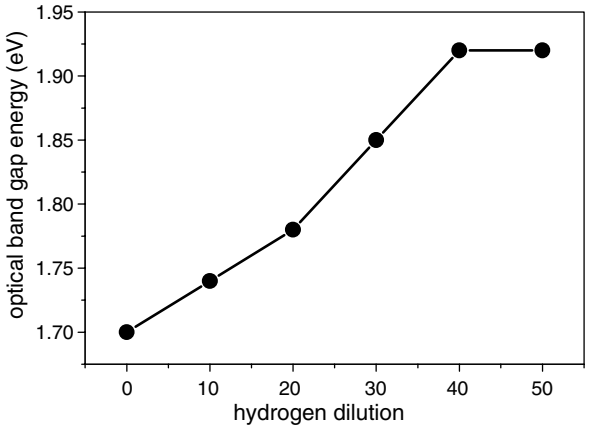

Fig. 4. Optical band gap energy of the deposited films as a function of the dilution.

regions are in Fig. 5. The spectral region at wavenumbers $<1300\,cm^{-1}$ is strongly influenced by the glass substrate and therefore wagging and bending absorption bands of Si:H bonds (Table 2) often used for the hydrogen content calculations are disqualified.

Therefore, the attention was focused on the broad absorbance bands at $\sim$2000–2100 cm^{-1} (Fig. 6) assigned to silicon to hydrogen bonds, that actually represents the convolution of overlapping stretching vibrations at $\sim2000\,cm^{-1}$ and $\sim2090\,cm^{-1}$ that give information about how hydrogen is bonded. The dominant peak centered at $\sim2000\,cm^{-1}$ belongs to the monohydride SiH and peak centered at $\sim2090\,cm^{-1}$ is assigned to the dihydride SiH_2 or clustered hydrogen. Absorbance peaks plotted in Fig. 6 were smoothed, baseline corrected and deconvoluted by least squares fitting with Gaussian intensity distribution I as a function of the wavenumber $\bar{\nu}$. Integral intensities of two deconvoluted peaks are proportional to bonded atoms densities. Presence of SiH_x while $x > 1$ is common for material with microvoids. More loose SiH_2 bonds are typical for polycrystalline silicon.

Optical properties of polysilicon as a function of H microstructure are represented by microstructure factor $\mu = \frac{\int I_{SiH_2}(\bar{\nu})d\bar{\nu}}{\int I_{SiH_2}(\bar{\nu})d\bar{\nu}+\int I_{SiH}(\bar{\nu})d\bar{\nu}}$ which is commonly considered as a figure of merit of the quality of the films when being <10% (Stanowski and Schropp, 2001). The density of hydrogen atoms bonded to silicon is $N = A_x \int \frac{\alpha(\bar{\nu})}{\bar{\nu}} d\bar{\nu}$, where A_x is the proportionality constant for specific vibrational mode (Gracin et al., 1995; Pereyra and Carreno, 1998; van der Oever et al., 2003), $\alpha(\bar{\nu})$ is the wavenumber dependent absorption coefficient. Hydrogen concentration in atomic percent is $C = \frac{A_x}{N_{int}} \int \frac{\alpha(\bar{\nu})}{\bar{\nu}} d\bar{\nu}$. N_{int} is the total atomic density of the films ($5 \times 10^{22}\,cm^{-3}$ for c-Si). Microstructure factor and hydrogen concentration (calculated with the proportionality constant $A_x = 9 \times 10^{19}\,cm^{-2}$) as functions of the dilution are in Fig. 7(a). Hydrogen concentration declines with increasing dilution and thus with progressing crystallisation of the sample. We observed the apparent shift of the position of the absorption peak at $\sim2000\,cm^{-1}$ to higher wavenumbers with increasing dilution (Fig. 7(b)) similarly to Park and Rhee (Park and Rhee, 2001). The shift can be attributed to the increasing order in the silicon network and increasing crystalline fraction.

The regions marked by the pattern in Fig. 7 containing the intersections of plots at dilutions between 20 and 30 can be attributed to the amorphous-to-crystalline transition, thus to the protocrystalline (or "edge") material recommended for applications in photovoltaics (Collins et al., 2003; Kočka et al., 2004).

The ratio $r_s = \alpha_{2090}/\alpha_{2000}$ of the absorption coefficients at $2090\,cm^{-1}$ and $2000\,cm^{-1}$ is related to the film stress (Park et al., 1999). The compressive stress decreases the ratio $r_s = \alpha_{2090}/\alpha_{2000}$, while the tensile stress increases the ratio. For the samples under study it was discovered that increasing dilu-

Table 2
Characteristic vibrational modes of Si–H and Si–O bonds

	Mode assignment		Wavenumber (cm^{-1})
SiH_x ($x = 1, 2, 3$)	Wagging	Hydride	630–670
Si–O–Si	Stretching (weak)	Interstitial oxygen	780–800
SiH_x ($x = 1, 2, 3$)	Bending (weak)	Hydride	845–910
Si–O–Si	Asymmetric stretching	Interstitial oxygen	940–1030
SiH	Stretching	Monohydride	2000
SiH_2	Stretching	Dihydride	2090
Si–OH	Stretching	Silanol	3000–3700

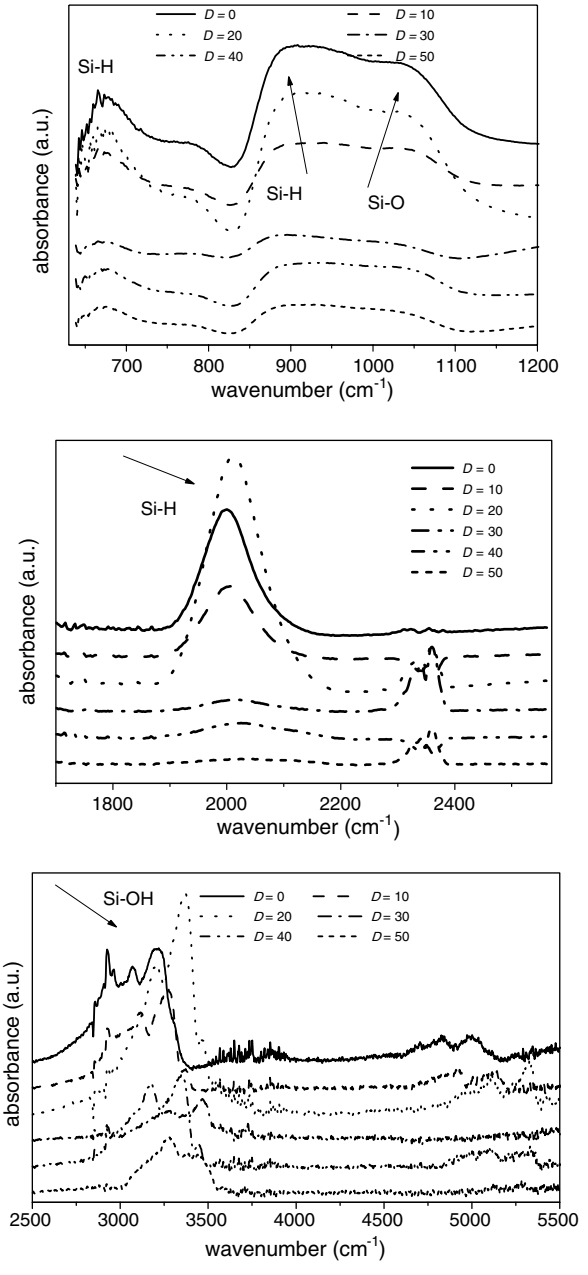

Fig. 5. IR absorbance spectra of the deposited films. The peak at $\sim$2350 cm^{-1} belongs to the atmospheric CO_2 coming from the measuring chamber of the spectrophotometer.

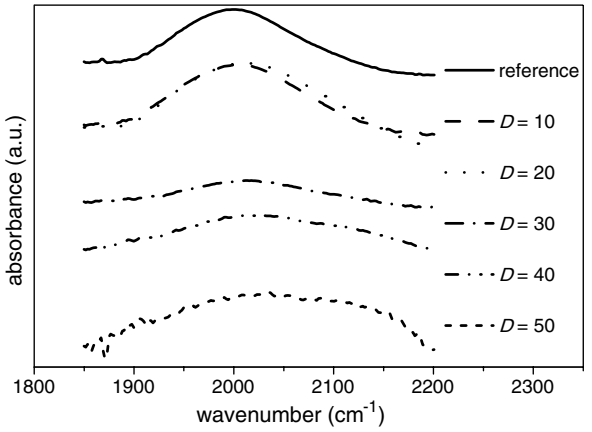

Fig. 6. Vibrational absorbance peaks assigned to the stretching vibrations of Si–H and Si–H_2 bonds measured by FTIR for the samples deposited under various dilutions D.

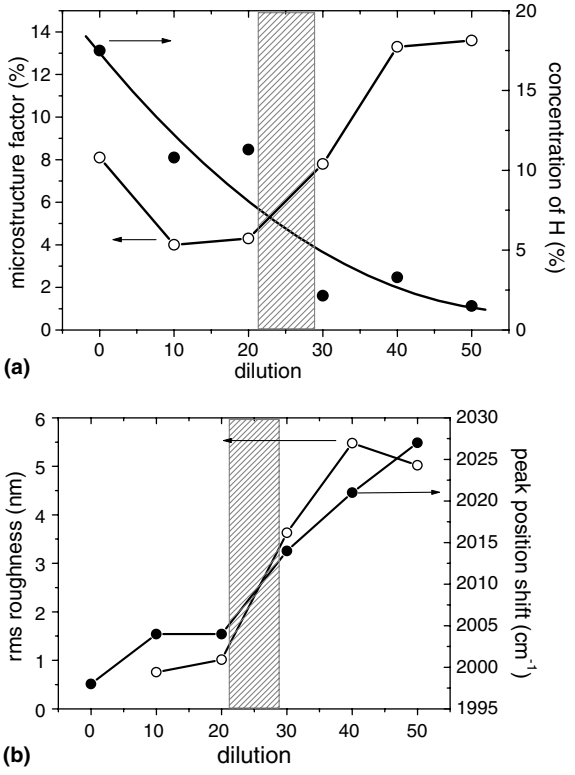

Fig. 7. The total bonded hydrogen concentration and the microstructure factor (a), the shift of the vibrational peak at $\sim$2000 cm^{-1} position and the rms surface roughness (b) as functions of the dilution. The patterned regions are attributed to the amorphous-to-crystalline transition.

tion increases the ratio r_s (Table 3) what means that polycrystalline films are under tensile stress. This is in agreement with the XRD analysis (Müllerová et al., 2005). As the hydrogen concentration drops with the dilution, the increase of the tensile stress is obviously not influenced by this decrease, but can be due to the increasing amount of collapsing SiH_2 bonds and voids and decreasing film density. This observation is similar to that already pointed by Wehrspohn et al. (Wehrspohn et al., 2000).

Table 3
Parameters related to the film stress (r_s) and oxygen content (c_O) according to FTIR study

	Dilution D	SiH_4 concentration (%)	r_s	c_O
Reference	0	100	0.0812	4.6
#1	10	9.1	0.0397	3.3
#2	20	4.8	0.0427	6.22
#3	30	3.2	0.0780	1.25
#4	40	2.4	0.1360	3.2
#5	50	2.0	0.1330	1.92

Another complication may originate from the detrimental oxygen contamination of Si:H films that usually results in conductivity changes and enhanced porosity of the samples (Persheyev et al., 2004). FTIR measurements show that all films are contaminated with certain amount of oxygen. This could be an effect of post-deposition oxidation by the exposure to the air. In the absorbance spectra the pronounced stretching vibrations of the interstitial oxygen in the O–Si–O bonds at $\sim$1000 cm^{-1} and about one order less intense surface vibrational features extended from 3000 cm^{-1} to 3800 cm^{-1} (Fig. 5) attributed to Si–OH species occur. The area under the broad absorption band of surface Si–OH groups called silanols at $\sim$3100 cm^{-1} can be regarded as the parameter c_O related to the oxygen concentration proportional to the surface oxygen density (Table 3). It reaches its maximum at $D \sim 20$ and then decreases. The same behaviour of interstitial oxygen was observed analysing the absorption band at $\sim$1000 cm^{-1}.

5. Conclusions

In Si:H PECVD deposition, remarkable changes in structure and optical properties of Si:H thin films due to the increasing hydrogen dilution of silane plasma were found. The samples prepared at the dilution under 20 are found to remain within the amorphous regime with the negligible surface roughness. The films prepared at $D \geqslant 30$ were detected as nanometer grain-sized polycrystalline Si under tensile stress with voids and grain boundaries passivated by hydrogen. Grains in the nanometer range exist within the surface features seen by AFM. The protocrystalline regime occurs between the dilutions 20 and 30. A high void fraction was verified by reducing refractive index with increasing dilution. The dilution favours the refractive index and optical band gap engineering. The optical band gap increases from 1.7 for the undiluted reference a-Si:H sample to 1.92 for the polycrystalline sample deposited under dilution 50. FTIR results show primarily monohydride SiH bonding with the progressing part of dihydride SiH_2 while the dilution rises. With increasing dilution and the crystallinity, the hydrogen concentration declines. In spite of the microstructure factor growing over 10% in the films at $D > 20$, the inevitable increasing presence of oxygen was surprisingly not observed.

Acknowledgements

This work was supported in part by the Slovak Grant Agency under Grants Nos. 2/4105/04, 2/4100/04 and by the Project of Research and Development LN00B084 of the Czech Ministry of Education, Youth and Sports. Dr. Nádaždy at the Institute of Physics, Slovak Academy of Sciences, Bratislava, Slovakia, is acknowledged for the sample preparation and Dr. Michalka at the International Laser Centre, Bratislava, Slovakia, for the AFM measurements.

References

Brügemann, R., Bronner, W., Hierzenberger, A., Schubert, M.B., Zrinscak, I., 1999. Electronic properties of hot-wire CVD and PECVD deposited nanocrystalline silicon. In: Marshall, J.M. (ed.), Thin film materials and devices—developments in science and technology, Singapore, 1–12.

Collins, R.W., Ferlauto, A.S., Ferreira, G.M., Chen, C., Koh, J., Koval, R.J., Lee, Y., Pearce, J.M., Wronski, C.R., 2003. Evolution of microstructure and phase in amorphous, protocrystalline, and microcrystalline silicon studied by real time spectroscopic ellipsometry. Solar Energ. Mater. Solar Cells 78 (1–4), 143–180.

Gracin, D., Radić, N., Desnica, U.V., Andreić, Ž., Balzar, D., 1995. Thermal stability of amorphous silicon–carbon alloys deposited by magnetron source. Fizika A 4 (2), 329–335.

Jurečka, S., Jurečková, M., Müllerová, J., 2003. Genetic algorithm approach to thin film optical parameters determination. Acta Phys. Slovaca 53 (3), 215–221.

Kočka, J., Fejfar, A., Mates, T., Fojtík, P., Dohnalová, K., Luterová, K., Stuchlík, J., Stuchlíková, H., Pelant, I., Rezek, B., Stemmer, A., Ito, M., 2004. The physics and technological aspects of the transition from amorphous to microcrystalline and polycrystalline silicon. Phys. Status Solidi 1 (5), 1097–1114.

Koval, R.C., Koh, J., Lu, Z., Jiao, L., Collins, R.W., Wronski, C.R., 1999. Performance and stability of Si:H *p-i-n* solar cells with *i*-layers prepared at the thickness-dependent amorphous-to-microcrystalline phase boundary. Appl. Phys. Lett. 75 (11), 1553–1555.

Müllerová, J., Jurečka, J., Šutta, P., 2005. Structural and optical studies of a-Si:H thin films: from amorphous to nanocrystalline silicon. Acta Phys. Slovaca 55 (3), 351–359.

Müllerová, J., Jurečka, S., Kučerová, A., 2003. Extraction of optical parameters of thin films from spectral measurements for design and optical performance of multilayer structures. Acta Phys. Slovaca 53 (2), 111–119.

Nádaždy, V., Durný, R., Thurzo, I., Pinčík, E., Nishida, A., Shimizu, J., Kumeda, M., Shimizu, T., 2002. Correlation between the results of charge deep-level transient spectroscopy and ESR techniques for undoped hydrogenated amorphous silicon. Phys. Rev. B 66, 195211-1–195211-8.

Park, Y.-B., Li, X., Rhee, S.-W., Park, D.-W., 1999. Remote plasma chemical vapour deposition of silicon films at low temperature with H_2 and He plasma gases. J. Phys. D: Appl. Phys. 32, 1955–1962.

Park, Y.-B., Rhee, S.-W., 2001. Microstructure and initial growth characteristics of the low temperature microcrystalline silicon films on silicon nitride surface. J. Appl. Phys. 90 (1), 217–221.

Pereyra, I., Carreno, M.N.P., 1998. The influence of "starving plasma" regime on carbon content and bonds in a-$Si_{1-x}C_x$:H thin films. J. Appl. Phys. 84 (5), 2371–2379.

Persheyev, S.K., O'Neill, K.A., Anthony, S., Rose, M.J., Smirnov, V., Reynolds, S., 2004. Metastability in undoped microcrystalline silicon thin films deposited by HWCVD. Mater. Res. Soc. Symp. Proc. 808, A9101–A9106.

Reynolds, S., Smirnov, V., Finger, F., Main, C., Carius, R., 2005. Transport and instabilities in microcrystallline silicon films. J. Optoelectron. Adv. Mater. 7 (1), 91–98.

Staebler, D.L., Wronski, C.R., 1977. Reversible Conductivity Changes in Discharge-Produced Amorphous Si. Appl. Phys. Lett. 31, 292–294.

Stanowski, B., Schropp, R.E.I., 2001. Hot-wire amorphous silicon thin-film transistors on glass. Thin Solid Films 383, 125–128.

van der Oever, P.J., Houston, I.J., van de Sanden, M.C.M., Kessels, W.M.M.M., 2003. Attenuated total reflection infrared spectroscopic study of hydrogenated amorphous and microcrystalline silicon film evolution. In: Proc. FLTP V, Frontier in Low Temperature Plasma Diagnostics V, Villaggio Cardigliano, Specchia, Italy, 263 – 265.

van Zutphen, A.J.M.M., Šutta, P., Tichelaar, F.D., von Keitz, A., Zeman, M., Metselaar, J.W., 2001. Structure of thin polycrystalline silicon films on ceramic substrates. J. Cryst. Growth 223, 332–340.

Wehrspohn, R.B., Deane, S.C., French, I.D., Gale, I., Hewett, J., Powell, M.J., 2000. Relative importance of Si–Si bond and Si–H bond for the stability of amorphous silicon thin films transistors. J. Appl. Phys. 87 (1), 144–154.

Wronski, C.R., Pearce, J.M., Koval, R.J., Ferlauto, A.S., Collins, R,W., 2002. Progress in amorphous silicon based solar cell technology. In: Proc. RIO 02—World Climate and Energy Event, 67–72.